Neoarchean oxygen-based nitrogen cycle en route to the Great Oxidation Event

Alice Pellerin[1*], Christophe Thomazo[1,3], Magali Ader[2], Camille Rossignol[4], Eric Siciliano Rego[5], Vincent Busigny[2], and Pascal Philippot[6,7]

[1]Laboratoire Biogéosciences, UMR CNRS 6282, Université de Bourgogne; Dijon, France
[2]Université Paris Cité, Institut de Physique du Globe de Paris, CNRS ; F-75005 Paris, France
[3]Institut Universitaire de France (IUF)
[4]Dipartimento di Scienze Chimiche e Geologiche, Università degli studi di Cagliari ; Italy
[5]Scripps Institution of Oceanography, Geosciences Research Division, UC San Diego, La Jolla, CA 92093, USA
[6]Géosciences Montpellier, Université de Montpellier, CNRS ; 34095 Montpellier, France
[7]Departamento de Geofísica, Instituto de Astronomia, Geofísica e Ciências Atmosféricas, Universidade de São Paulo ; Rua do Matão 1226, Cidade Universitária, São Paulo, 05508-090, Brazil
*Corresponding author. Email: alice.pellerin-lefebvre@u-bourgogne.fr

Summary paragraph

The nitrogen isotopic composition of sedimentary rocks ($\delta^{15}N$) can trace redox-dependent biological pathways and early Earth oxygenation[1,2]. However, there is no substantial change in the sedimentary $\delta^{15}N$ record across the Great Oxidation Event ~2.45 Ga[3], a prominent redox change. This argues for a temporal decoupling between the emergence of the first oxygen-based oxidative pathways of the nitrogen cycle and the accumulation of atmospheric oxygen after ~2.45 Ga[3]. The transition between both states displays strongly positive $\delta^{15}N$ values (10-50‰) in rocks deposited between 2.8 and 2.6 Ga, but their origin and spatial extent remains uncertain[4,5]. Here we report strongly positive $\delta^{15}N$ values (> 30‰) in the ca. 2.68 Ga old shallow to deep marine sedimentary deposit of the Serra Sul Formation[6], Amazonian Craton, Brazil. Our findings are best explained by regionally variable extents of ammonium oxidation to N_2 or N_2O tied to a cryptic oxygen cycle, implying that oxygenic photosynthesis was operating 2.7 Ga ago. Molecular oxygen production likely shifted the redox potential so that an intermediate N cycle based on ammonium oxidation developed before nitrate accumulation in surface waters. We propose to name this period, when strongly positive nitrogen isotopic compositions are superimposed on the usual range of Precambrian $\delta^{15}N$ values, the Nitrogen Isotope Event (NIE). We suggest that it marks the earliest steps of the biogeochemical reorganizations that led to the Great Oxidation Event.

N isotopes record water column oxidation

Nitrogen is an essential nutrient for the biosphere, exerting a strong control on biological productivity through the availability of its "fixed" bioavailable forms, including ammonium (NH_4^+), nitrite (NO_2^-) and nitrate (NO_3^-), which can all be readily uptaken by primary producers. The nitrogen isotope composition ($\delta^{15}N=[(^{15}N/^{14}N)_{sample}/(^{15}N/^{14}N)_{standard}]-1$, where the standard is N_2 in air) of these nitrogen forms is controlled by microbially-mediated metabolic reactions,

most of them sensitive to the redox state of the water column. When assimilated, N species transfer their isotope signature to the organic matter, which can subsequently be preserved in sedimentary rocks[7]. Nitrogen isotopes in the sedimentary record thus represent an ideal tool for investigating the joint temporal evolution of surface environments oxidation and primary productivity.

Despite being largely present in the atmosphere as gaseous N_2 ($\delta^{15}N$=0‰), nitrogen in this form can only be assimilated by diazotrophs, nitrogenase-bearing prokaryotes capable of biological N_2 fixation. Fractionation imparted by biological N_2 fixation with classical Mo-based nitrogenase ranges from -2‰ to +2‰, whereas alternative nitrogenase using Fe or V as cofactors can impart negative fractionation as large as -8‰[8]. The mineralization of organic matter derived from diazotrophic activity in the water column or in sediments, namely ammonification[9], provides most of the bioavailable nitrogen to the biosphere as ammonium (NH_4^+) without significant isotope fractionation[10]. In anoxic conditions, ammonium released during organic matter mineralization is rapidly and quantitatively assimilated into biomass. Hence, even if ammonium assimilation preferentially incorporates ^{14}N, its fractionation is rarely expressed in the sedimentary record. In oxic conditions, ammonium can either be assimilated or nitrified to nitrite and nitrate, enriching residual ammonium by up to +35‰[11]. In modern environments, where oxygen levels are in excess, ammonium is oxidized quantitatively, preventing the fractionation associated with ammonium oxidation from being expressed. Nitrite and nitrate are in turn assimilated by photosynthetic organisms or biologically reduced, either through denitrification or anaerobic ammonium oxidation (anammox) in dysoxic and anoxic conditions[9,12]. Denitrification and anammox are the major oceanic sinks of fixed nitrogen, releasing N_2O or N_2 back to the atmosphere. Both of these sinks impart a large nitrogen isotope fractionation of around +30‰[9], leaving behind ^{15}N-enriched residual nitrate that can be uptaken by primary producers and subsequently transferred to the sediments. In modern environments, and by extension any sediment deposited under oxic conditions, $\delta^{15}N$ values around +5‰ are interpreted to reflect the balance between N_2 fixation inputs and denitrification/anammox outputs from the water column and surface sediments.

A unique Neoarchean $\delta^{15}N$ record

The secular evolution of sedimentary $\delta^{15}N$ values shifts from a mode of +2‰ between 3.8 and 2.8 Ga in the Archean to a mode of +5‰ between 2.5 and 1.8 Ga[1]. Based on this framework, and assuming that (i) atmospheric N_2 isotope composition ($\delta^{15}N_{N2}$=0‰) has remained stable since the Paleoarchean[13,14], and that (ii) N_2 assimilation through biological nitrogen fixation provides the fixed-N source needed to sustain biomass production since at least 3.2 Ga[2,15], this evolution has mostly been attributed to a major change in the nitrogen biogeochemical cycle. From being ammonium-dominated in the essentially anoxic Archean oceans and lakes, including in their surface waters, the N-biogeochemical cycle would have evolved to nitrate-dominated after 2.5 Ga in transiently oxic surface waters[1,2,16–20]. Intriguingly, there is no significant change in the sedimentary $\delta^{15}N$ record across the Great Oxidation Event (GOE) (e.g.[3]; Figure 1A), which is widely considered as the most prominent redox change in Earth history. This argues for a temporal decoupling between the emergence of the first oxygen-based oxidative pathway of the biogeochemical nitrogen cycle and the accumulation of free oxygen in the atmosphere after 2.45 Ga.

The transition between both states, occurring at the end of the Archean, displays strongly positive $\delta^{15}N$ values (between +10 and +50‰, Figure 1A) recorded in sedimentary rocks deposited between 2.8 and 2.6 Ga in at least 5 different locations[4,5,21–24] (Supplementary Table 1). They have been interpreted in various ways (Supplementary Table 1), including: (i) metamorphic alteration of the original isotopic signature[21], (ii) a ^{15}N-enriched atmospheric reservoir derived from chondrite-like material[22,23], (iii) the onset of an oxidative pathway in the nitrogen cycle, arguing for the presence of cryptic oxygen in an otherwise anoxic ocean, prior to the oxygenation of the atmosphere[4], and more recently (iv) NH_3 degassing from alkaline waters of restricted lacustrine environments[5,24]. This latter hypothesis has gained momentum because the most positive $\delta^{15}N$ values reported so far are associated with extreme negative $\delta^{13}C_{org}$ values[25] (Figure 1B) and stem from the Tumbiana Formation in the Pilbara Craton, now firmly demonstrated to have been deposited in an alkaline lake[26]. Yet it implies that the relative synchronicity of these positive $\delta^{15}N$ values and their occurrence right at the transition between the two $\delta^{15}N$ distribution modes would have happened incidentally.

Here we take the opportunity of the discovery of a new occurrence of extreme $\delta^{15}N$ and $\delta^{13}C_{org}$ values from the Serra Sul Formation, Amazonian Craton, Brazil, deposited between 2684 ± 10 Ma and 2627 ± 11 Ma[6,27,28], to reassess the significance of these positive $\delta^{15}N$ values. This Neoarchean formation is representative of a marine shelf system with a sedimentary sequence ranging from shallow to deep-water environments with slope instabilities and debris flow[6] (Extended Data). Two drill cores intercepting the Serra Sul Formation, GT13 and GT16 (Extended Data, Extended Data Figure 1), were studied. They display polygenic and flat-pebble conglomerates interbedded with fine-grained siliciclastic sediments[6] indicating the presence of sediments from both shallow and deep water environments, respectively (Figure 2; Extended Data; Extended Data Figure 1).

Organic carbon and nitrogen concentrations and isotopic compositions for the two studied drill cores are reported in Table 1, Figure 1 and Figure 2. For both drill cores, $\delta^{15}N$ values are markedly positive, from +13.9 to +37.5‰, with mean values of +32.9 ± 3.4‰ (n = 11) and +24.6 ± 6.0‰ (n = 13) for GT13 and GT16, respectively. $\delta^{13}C_{org}$ values are ^{13}C-depleted, ranging from -30.4 to -51.8‰, with comparable mean values (-40.0 ± 1.2‰ for GT13 and -44.1 ± 6.1‰ for GT16). Overall, carbon and nitrogen concentrations and isotopic compositions appear relatively homogeneous throughout drill core GT13, compared to the more scattered signal in drill core GT16. No variations were observed with respect to lithological features or facies changes (Figure 2).

Defining a Nitrogen Isotope Event (NIE)

Overall, despite different geological settings, depositional environments, and paleogeography, this new occurrence of a paired $\delta^{15}N$-$\delta^{13}C_{org}$ excursion recorded in the Amazonian Craton is within the range of the one reported in the Pilbara Craton, suggesting that these extremely positive $\delta^{15}N$ values are inherent to the 2.8-2.6 Ga time interval. Importantly, since these extreme values coexist with less extreme values (Figure 1; i.e. $\delta^{15}N$ from -1 to +6‰[1]) in other Neoarchean basins at sub-greenschist facies, regional controls must be at play. This extreme range of $\delta^{15}N$ values seems to be unique in the geological record and we propose to single it out as the Nitrogen Isotope Event (NIE).

In order to investigate the nature of this NIE, we can first focus on the significance of the extremely positive $\delta^{15}N$ values, starting with the reassessment of previously proposed hypotheses. The hypothesis of a ^{15}N-enriched atmospheric reservoir derived from chondrite-like material[22,23] can be ruled out because (i) such a contribution from ^{15}N-enriched extraterrestrial material should be observed well before 2.8 Ga (Figure 1) and (ii) the abundance of $\delta^{15}N$ extreme values should decrease with time, in contrast with the unique sharp peak recorded between 2.8 and 2.6 Ga (Figure 1). Furthermore, while micrometeorites have been reported in the Tumbiana Formation[29], there is no evidence for contribution of extraterrestrial material within the Serra Sul Formation.

Several lines of evidence can also be used to rule out metamorphic alteration as the mechanism responsible for extreme $\delta^{15}N$ values, at least in the Serra Sul Formation. Indeed, known diagenetic, metamorphic or hydrothermal processes rarely enrich sedimentary nitrogen in ^{15}N to an extent of more than 10‰[1,30], while $\delta^{15}N$ values in the Serra Sul Formation range from +14 to +38‰. Moreover, metamorphism in the Serra Sul Formation does not exceed the greenschist facies (Supplementary Information), implying a negligible impact of post-depositional processes on the studied samples[31,32]. Last but not least, no correlations were observed between Total N content (TN) and $\delta^{15}N$ ($R^2 < 0.14$), Total Organic Carbon content (TOC)/TN ratios and $\delta^{15}N$ ($R^2 < 0.20$), or $\delta^{15}N$ and $\delta^{13}C_{org}$ ($R^2 < 0.26$) (Extended Data Figure 2).

Finally, the hypothesis of positive ammonium $\delta^{15}N$ values resulting from NH_3 degassing at high pH[5,24] proposed as an explanation for extreme $\delta^{15}N$ values in the 2.72 Ga Tumbiana Formation does not hold for the Serra Sul Formation, unless the ocean also had a high pH at the time. Indeed, at pH > 9.2, NH_4^+ dissociates to NH_3, which can degas to the atmosphere with a strong isotope fractionation (+45‰ at 23°C[33]). When assimilated, the residual ^{15}N-enriched NH_4^+ transfers its signature to the organic matter, which can subsequently be preserved in sedimentary rocks. Although such strong fractionations have never been recorded in modern alkaline environments, this hypothesis is well suited for the Tumbiana Formation, which was deposited in a restricted lacustrine setting with a substratum made of alkaline rocks[26]. The abiotic loss of nitrogen from the water column caused by ammonia degassing also provides a consistent explanation for the low TN and high TOC/TN of sediments from this formation[5]. However, samples from the Serra Sul Formation analyzed here neither show a strong TN depletion compared to other Neoarchean sedimentary rocks, nor any evidence of being deposited under a highly alkaline water column. They are representative of shallow to deep marine depositional environments, with neither evaporitic facies nor carbonates (Supplementary Information). If we assume that the ocean pH at the time was lower than 9.2[34], NH_3 degassing cannot solely account for the extremely positive $\delta^{15}N$ values of the Serra Sul Formation.

Accordingly, none of these hypotheses can explain the NIE. The only one left to explore is a change in the biological nitrogen cycle, which is shown from today's sedimentary record[35] and likely also in the Precambrian[1], to be regionally controlled.

A transitional state in the N cycle

Only a few metabolic pathways of the N-biogeochemical cycle can lead to a ^{15}N-enrichment of fixed nitrogen species. N_2 fixation with classic Fe-Mo nitrogenase does not impart any significant fractionation[9], and Fe-Fe or Fe-V alternative nitrogenases generate organic matter with a negative $\delta^{15}N$[8]. Ammonification has a negligible impact on the $\delta^{15}N$[9]. Partial biological assimilation of NH_4^+ can enrich organic matter in ^{14}N ($\varepsilon \approx$ -4‰ to -27‰[36]) if the pool of ammonium is progressively distilled but not quantitatively consumed[37]. However, the expected distribution of $\delta^{15}N$ values following partial assimilation alone should be centered around 0‰, displaying both the upwelled ^{15}N-depleted and the sinking ^{15}N-enriched pools of ammonium. This mechanism has been proposed to explain a single set of Neoarchean $\delta^{15}N$ values[38], yet the two complementary fractions have never been recovered from the same study site. Our reported $\delta^{15}N$ data from the Serra Sul Formation are centered around +28‰, with no negative values (Figure 2). Therefore, they are inconsistent with the distillation of an NH_4^+ reservoir by a simple assimilation process. None of the above-mentioned pathways can produce the extremely positive $\delta^{15}N$ values recorded in the Serra Sul Formation. An oxidative pathway that strongly fractionates N isotopes must therefore have been at play.

The strongly fractionating metabolism commonly considered for the moderately positive $\delta^{15}N$ values recorded from 2.5 Ga onwards is non quantitative denitrification[16,17,19,20], which in the modern ocean occurs in dysoxic parts of the water column. It requires both nitrification and a large and consistently oxic surface water layer where nitrate can accumulate. In this case, it is the isotope composition of the enriched residual nitrate that is expressed and recorded in the sediments. Although denitrification can induce isotope fractionation by as much as 30‰ in nitrate-replete conditions[39], the observed range of $\delta^{15}N$ values should be significantly smaller, as it depends on the isotope mass balance between N_2-fixation and denitrification in Oxygen Minimum Zones (OMZs) or sediments. As an example, in the modern ocean where nitrate is stable both in the photic zone and in deeper waters, and thus not fully denitrified, $\delta^{15}N$ values only reach up to +15‰ in OMZs[9,35,39].

For both drill core samples of the Serra Sul Formation, ammonium is expected to be the dominant fixed nitrogen species[40]. We thus propose a scenario where the mechanism responsible for the positive $\delta^{15}N$ values is ammonium oxidation to N_2, N_2O, or NO_2^-, tied to a cryptic oxygen cycle. Ammonium oxidation isotope fractionation can reach up to +55‰ when ammonium is co-oxidized with methane by methanotrophs[41] and up to +38‰ when ammonium is oxidized by ammonium-oxidizing bacteria and archaea[42]. Importantly, as for denitrification, the isotope expression of this oxidative pathway requires ammonium oxidation to be non quantitative.

In the anoxic ocean of the early Neoarchean, ammonium oxidation can only take place in the photic zone where photosynthesis occurs and generates the electrochemical potential necessary to oxidize ammonium. In this photic zone, ammonium oxidation must be in competition with ammonium assimilation, since photosynthetizers require N for their growth. From there, several cases can be envisioned. If photosynthesis hardly generates the necessary oxidants for ammonium oxidation, then ammonium is essentially assimilated by photosynthetizers and, depending on its rate of assimilation, its ^{15}N-enrichment will be low to null. ^{15}N-depletion can even happen, which may explain the slightly negative $\delta^{15}N$ values reported during the NIE[38]. If photosynthesis generates enough oxidants to oxidize much of the ammonium before it can be assimilated, ^{15}N-enrichments will also be low or null as N would be supplied by N_2-fixation. As a result, a nitrogen cycle comprising the different pathways of ammonium oxidation to

gaseous N-species continuously escaping the system can generate all the range of $\delta^{15}N$ values reported during the NIE, from mildly negative to extremely positive depending on regional controls on primary productivity and ammonium supply.

In summary, similarly to nitrate-dominated environments where $\delta^{15}N_{NO3-}$ values are regionally controlled (ranging from 0 to 15‰) and depend on the mass and isotope balance between N sources (N_2-fixation and nitrate supply) and N sinks (denitrification in the water column, in the sediments and nitrate assimilation), in an ammonium-dominated environment, the $\delta^{15}N_{NH4}$ values would depend on the mass and isotope balance between N_2-fixation, ammonium supply, ammonium oxidation and ammonium assimilation. The extreme range of $\delta^{15}N$ values recorded in the Tumbiana Formation is even better explained by ammonia degassing occurring alongside ammonium oxidation, which together could drive $\delta^{15}N$ values up to +50‰.

From the NIE to the GOE

For such a transitional state to occur during the Neoarchean, photosynthesis must have been generating oxidants able to oxidize ammonium into volatile gaseous species. Most metabolic pathways oxidizing ammonium need O_2. Even canonical anaerobic ammonium oxidation (anammox) requires the presence of nitrite, which cannot be produced without O_2[43]. In a fully anoxic world, in the absence of oxygenic photosynthesis, only the Feammox reaction has been suggested as a biological mechanism associated with ammonium oxidation[44]. However, this pathway has been substantiated for iron-rich depositional environments and associated with only slightly positive $\delta^{15}N$ values[44].

Dioxygen is therefore necessary to account for ammonium oxidation during the NIE. The preservation of a sulfur mass independent fractionation signal in both the Serra Sul and Tumbiana sediments[45,46] indicates, however, that free O_2 was not accumulating in the ocean and atmosphere at that time. Free O_2 must have been present at a low level but in sufficient amounts to fuel ammonium oxidation. Indeed, in modern nitrite-rich anoxic marine zones, ammonium oxidation occurs at nanomolar oxygen concentrations, compatible with anoxic surrounding waters[47]. The overall low levels of O_2 would also prevent the accumulation of nitrate if any was formed, which would have been quantitatively converted into N_2 or N_2O.

This intermediate state of the N-cycle would have ended progressively as O_2 supply in the photic zone surpassed ammonium supply. With increasing O_2 concentrations, ammonium oxidation would have proceeded up to nitrate production in dysoxic surface water masses. As their size grew, these dysoxic surface water masses became connected, and extended deeper than the photic zone. Nitrate was able to accumulate, turning the N-cycle to a new steady state where denitrification and anammox became the main drivers of the $\delta^{15}N$ sedimentary record.

We conclude that the extreme range of nitrogen isotope signatures recorded in the 2.8-2.6 Ga time interval reflect micro-aerobic conditions prone to the emergence of ammonium oxidation. The NIE would thus mark the emergence of biological oxidative nitrogen cycling in surface oceans transitioning from fully anoxic to coexisting anoxic and dysoxic water masses and might underline one of the very first steps of the GOE.

REFERENCES

1. Ader, M. *et al.* Interpretation of the nitrogen isotopic composition of Precambrian sedimentary rocks: Assumptions and perspectives. *Chem. Geol.* **429**, 93–110 (2016).

2. Stüeken, E. E., Kipp, M. A., Koehler, M. C. & Buick, R. The evolution of Earth's biogeochemical nitrogen cycle. *Earth-Sci. Rev.* **160**, 220–239 (2016).

3. Lyons, T. W., Reinhard, C. T. & Planavsky, N. J. The rise of oxygen in Earth's early ocean and atmosphere. *Nature* **506**, 307–315 (2014).

4. Thomazo, C., Ader, M. & Philippot, P. Extreme 15N-enrichments in 2.72-Gyr-old sediments: evidence for a turning point in the nitrogen cycle. *Geobiology* **9**, 107–120 (2011).

5. Stüeken, E. E., Buick, R. & Schauer, A. J. Nitrogen isotope evidence for alkaline lakes on late Archean continents. *Earth Planet. Sci. Lett.* **411**, 1–10 (2015).

6. Rossignol, C. *et al.* Stratigraphy and geochronological constraints of the Serra Sul Formation (Carajás Basin, Amazonian Craton, Brazil). *Precambrian Res.* **351**, 105981 (2020).

7. Altabet, M. A. & Francois, R. Sedimentary nitrogen isotopic ratio as a recorder for surface ocean nitrate utilization. *Glob. Biogeochem. Cycles* **8**, 103–116 (1994).

8. Zhang, X., Sigman, D. M., Morel, F. M. M. & Kraepiel, A. M. L. Nitrogen isotope fractionation by alternative nitrogenases and past ocean anoxia. *Proc. Natl. Acad. Sci.* **111**, 4782–4787 (2014).

9. Sigman, D. M., Karsh, K. L. & Casciotti, K. L. Nitrogen Isotopes in the Ocean. *Encycl. Ocean Sci.* 40–54 (2009) doi:https://doi.org/10.1016/B978-012374473-9.00632-9.

10. Möbius, J. Isotope fractionation during nitrogen remineralization (ammonification): Implications for nitrogen isotope biogeochemistry. *Geochim. Cosmochim. Acta* **105**, 422–432 (2013).

11. Mariotti, A. *et al.* Experimental determination of nitrogen kinetic isotope fractionation: Some principles; illustration for the denitrification and nitrification processes. *Plant Soil* **62**, 413–430 (1981).

12. Dalsgaard, T. & Thamdrup, B. Factors Controlling Anaerobic Ammonium Oxidation with Nitrite in Marine Sediments. *Appl. Environ. Microbiol.* (2002) doi:10.1128/AEM.68.8.3802-3808.2002.

13. Nishizawa, M., Sano, Y., Ueno, Y. & Maruyama, S. Speciation and isotope ratios of nitrogen in fluid inclusions from seafloor hydrothermal deposits at ~ 3.5 Ga. *Earth Planet. Sci. Lett.* **254**, 332–344 (2007).

14. Marty, B., Zimmermann, L., Pujol, M., Burgess, R. & Philippot, P. Nitrogen Isotopic Composition and Density of the Archean Atmosphere. *Science* **342**, 101–104 (2013).

15. Stüeken, E. E., Buick, R., Guy, B. M. & Koehler, M. C. Isotopic evidence for biological nitrogen fixation by molybdenum-nitrogenase from 3.2 Gyr. *Nature* **520**, 666–669 (2015).

16. Kipp, M. A., Stüeken, E. E., Yun, M., Bekker, A. & Buick, R. Pervasive aerobic nitrogen cycling in the surface ocean across the Paleoproterozoic Era. *Earth Planet. Sci. Lett.* **500**, 117–126 (2018).

17. Koehler, M. C., Buick, R., Kipp, M. A., Stüeken, E. E. & Zaloumis, J. Transient surface ocean oxygenation recorded in the ~2.66-Ga Jeerinah Formation, Australia. *Proc. Natl. Acad. Sci.* **115**, 7711–7716 (2018).

18. Zerkle, A. L. *et al.* Onset of the aerobic nitrogen cycle during the Great Oxidation Event. *Nature* **542**, 465–467 (2017).

19. Garvin, J., Buick, R., Anbar, A. D., Arnold, G. L. & Kaufman, A. J. Isotopic Evidence for an Aerobic Nitrogen Cycle in the Latest Archean. *Science* **323**, 1045–1048 (2009).

20. Godfrey, L. V. & Falkowski, P. G. The cycling and redox state of nitrogen in the Archaean ocean. *Nat. Geosci.* **2**, 725–729 (2009).

21. Beaumont, V. & Robert, F. Nitrogen isotope ratios of kerogens in Precambrian cherts: a record of the evolution of atmosphere chemistry? *Precambrian Res.* **96**, 63–82 (1999).

22. Jia, Y. & Kerrich, R. Nitrogen 15–enriched Precambrian kerogen and hydrothermal systems. *Geochem. Geophys. Geosystems* **5**, (2004).

23. Kerrich, R., Jia, Y., Manikyamba, C. & Naqvi, S. M. Secular variations of N-isotopes in terrestrial reservoirs and ore deposits. *Geol. Soc. Am. Bull.* **198**, (2006).

24. Stüeken, E. E. *et al.* Environmental niches and metabolic diversity in Neoarchean lakes. *Geobiology* **15**, 767–783 (2017).

25. Hayes, J. M. Global methanotrophy at the Archean-Proterozoic transition. *Early Life Earth Nobel Symp. No 84* 220–236 (1994).

26. Awramik, S. M. & Buchheim, H. P. A giant, Late Archean lake system: The Meentheena Member (Tumbiana Formation; Fortescue Group), Western Australia. *Precambrian Res.* **174**, 215–240 (2009).

27. Rossignol, C. *et al.* Unraveling one billion years of geological evolution of the southeastern Amazonia Craton from detrital zircon analyses. *Geosci. Front.* (2021) doi:10.1016/j.gsf.2021.101202.

28. Perelló, J., Zulliger, G., García, A. & Creaser, R. A. Revisiting the IOCG geology and age of Alemão in the Igarapé Bahia camp, Carajás province, Brazil. *J. South Am. Earth Sci.* **124**, 104273 (2023).

29. Tomkins, A. G. *et al.* Ancient micrometeorites suggestive of an oxygen-rich Archaean upper atmosphere. *Nature* **533**, 235–238 (2016).

30. Stüeken, E. E., Boocock, T. J., Robinson, A., Mikhail, S. & Johnson, B. W. Hydrothermal recycling of sedimentary ammonium into oceanic crust and the Archean ocean at 3.24 Ga. *Geology* **49**, 822–826 (2021).

31. Figueiredo e Silva, R. C., Lobato, L. M., Zucchetti, M., Hagemann, S. & Vennemann, T. Geotectonic signature and hydrothermal alteration of metabasalts under- and overlying the giant Serra Norte iron deposits, Carajás mineral Province. *Ore Geol. Rev.* **120**, 103407 (2020).

32. Martins, P. L. G. *et al.* Low paleolatitude of the Carajás Basin at ~2.75 Ga: Paleomagnetic evidence from basaltic flows in Amazonia. *Precambrian Res.* **365**, 106411 (2021).

33. Li, L., Lollar, B. S., Li, H., Wortmann, U. G. & Lacrampe-Couloume, G. Ammonium stability and nitrogen isotope fractionations for NH4+–NH3(aq)–NH3(gas) systems at 20–70°C and pH of 2–13: Applications to habitability and nitrogen cycling in low-temperature hydrothermal systems. *Geochim. Cosmochim. Acta* **84**, 280–296 (2012).

34. Halevy, I. & Bachan, A. The geologic history of seawater pH. *Science* **355**, 1069–1071 (2017).

35. Tesdal, J.-E., Galbraith, E. & Kienast, M. Nitrogen isotopes in bulk marine sediment: Linking seafloor observations with subseafloor records. **10**, (2013).

36. Hoch, M. P., Fogel, M. L. & Kirchman, D. L. Isotope fractionation associated with ammonium uptake by a marine bacterium. *Limnol. Oceanogr.* **37**, 1447–1459 (1992).

37. Papineau, D. *et al.* High primary productivity and nitrogen cycling after the Paleoproterozoic phosphogenic event in the Aravalli Supergroup, India. *Precambrian Res.* **171**, 37–56 (2009).

38. Yang, J. *et al.* Ammonium availability in the Late Archaean nitrogen cycle. *Nat. Geosci.* **12**, 553–557 (2019).

39. Saitoh, M. *et al.* Nitrogen Isotope Record From a Mid-oceanic Paleo-Atoll Limestone to Constrain the Redox State of the Panthalassa Ocean in the Capitanian (Late Guadalupian, Permian). *Paleoceanogr. Paleoclimatology* **38**, e2022PA004573 (2023).

40. Canfield, D. E., Glazer, A. N. & Falkowski, P. G. The Evolution and Future of Earth's Nitrogen Cycle. *Science* **330**, 192–196 (2010).

41. Mandernack, K. W., Mills, C. T., Johnson, C. A., Rahn, T. & Kinney, C. The δ15N and δ18O values of N2O produced during the co-oxidation of ammonia by methanotrophic bacteria. *Chem. Geol.* **267**, 96–107 (2009).

42. Casciotti, K. L. Inverse kinetic isotope fractionation during bacterial nitrite oxidation. *Geochim. Cosmochim. Acta* **73**, 2061–2076 (2009).

43. Grotzinger, J. P. & Kasting, J. F. New Constraints on Precambrian Ocean Composition. *J. Geol.* **101**, 235–243 (1993).

44. Pellerin, A. *et al.* Iron-mediated anaerobic ammonium oxidation recorded in the early Archean ferruginous ocean. *Geobiology* **21**, 277–289 (2023).

45. Bouyon, A. *et al.* Multiple sulfur isotope record from the Precambrian of South America shows an unusual trend. **2018**, V31B-04 (2018).

46. Thomazo, C., Ader, M., Farquhar, J. & Philippot, P. Methanotrophs regulated atmospheric sulfur isotope anomalies during the Mesoarchean (Tumbiana Formation, Western Australia). *Earth Planet. Sci. Lett.* **279**, 65–75 (2009).

47. Ulloa, O., Canfield, D. E., DeLong, E. F., Letelier, R. M. & Stewart, F. J. Microbial oceanography of anoxic oxygen minimum zones. *Proc. Natl. Acad. Sci.* **109**, 15996–16003 (2012).

Figure 1. Compilation of paired Precambrian sedimentary $\delta^{15}N$ (a) and $\delta^{13}C_{org}$ (b) data, including all lithologies. The different colours represent the various metamorphic grades (lower than greenschist (light green), greenschist (medium green), higher than greenschist (dark green) facies). The studied samples are represented by circled red dots. They experienced only limited metamorphic conditions, not higher than greenschist facies.

Figure 2. Carbon and nitrogen geochemical and isotopic profiles for drill cores GT13 and GT16. Stratigraphic logs simplified from ref [6]. Dotted lines correspond to mean values. Error bars for $\delta^{15}N$ measurements represent s.d.

Table 1. Data featuring drill core ID, sample depth (m), TOC (wt. %, whole rock), TN (ppm, wholerock), TOC/TN, $\delta^{13}C_{org}$ (‰ vs. PDB), and $\delta^{15}N_{bulk}$ (‰ vs. air), for all samples analyzed along the GT13 and GT16 drill cores. Standard deviation (SD) and number of replicates (Nb repl.) are given for all parameters.

Drill core	**Depth (m)**	**TOC (wt. %)**	SD	Nb repl.	**TN (ppm)**	SD	Nb repl.	**TOC/TN**	**$\delta^{13}C_{org}$ (‰ vs. PDB)**	SD	Nb repl.	**$\delta^{15}N_{bulk}$ (‰ vs. air)**	SD	Nb repl.
GT13	211.45	0.42	0.108	2	32	5	2	132	-42.5	0.23	2	30.9	0.4	2
GT13	229.27	0.45	0.009	2	46		1	97	-40.2	0.05	2	34.2		1
GT13	237.735	0.34	0.006	2	32	2	2	107	-40.0	0.05	2	32.3	1.6	2
GT13	247.82	0.52	0.025	2	39		1	133	-40.5	0.23	2	29.2		1
GT13	258.165	0.38	0.013	2	31		1	121	-40.0	0.07	2	35.5		1
GT13	266.32	0.38	0.010	2	32		1	119	-37.9	0.08	2	37.5		1
GT13	277.175	0.38	0.015	2	36		1	106	-39.0	0.04	2	35.3		1
GT13	287.305	0.33	0.004	2	38		1	88	-40.0	0.18	2	28.7		1
GT13	301.81	0.65	0.015	2	39		1	167	-39.3	0.19	2	37.0		1
GT13	306.175	0.58	0.001	2	43	1	2	135	-41.1	0.07	2	33.2	0.1	2
GT13	319.46	0.42	0.009	2	46		1	92	-39.8	0.08	2	27.7		1
GT16	122.05	0.13		1	25		1	51	-43.1		1	27.4		1
GT16	152.775	0.06	0.003	2	11	1	2	54	-41.4	0.21	2	20.2	0.4	2
GT16	159.885	0.02	0.002	2	23		1	8	-30.4	0.08	2	23.6		1
GT16	166.05	0.12	0.000	2	20		1	61	-44.6	0.01	2	34.6		1
GT16	195.97	0.13	0.002	2	8		1	166	-48.6	0.07	2	20.4		1
GT16	208.61	0.24	0.001	2	26		1	91	-51.8	0.03	2	14.9		1
GT16	224.11	0.21	0.002	2	18		1	115	-49.9	0.52	2	30.8		1
GT16	234.725	0.25	0.024	2	27	3	2	94	-50.0	1.73	2	28.8	3.5	2
GT16	244.845	0.13	0.002	2	8		1	167	-48.5	0.21	2	13.9		1
GT16	290.835	0.03	0.000	2	22		1	14	-36.4	0.48	2	25.8		1
GT16	312.005	0.09	0.001	2	26		1	35	-46.3	0.09	2	24.6		1
GT16	324.595	0.14	0.010	2	22	4	2	62	-43.0	0.67	2	27.5	3.1	2
GT16	348.805	0.04	0.007	2	14		1	27	-39.6	0.54	2	27.6		1

METHODS

Sampling. Twenty-four samples were chosen along the two studied drill cores (11 samples for drill core GT13 and 13 samples for drill core GT16) according to their organic matter content (TOC>0.02% in the digestion residue), that mostly reflects their potential in containing enough nitrogen for analysis.

Chemical treatment prior to C and N analyses. Samples were first crushed into powder using a ring and puck mill in order to obtain sample powder smaller than 60 μm. Carbonate-free residues were obtained by mixing sample powders with 6N HCl for two successive digestion steps: first at room temperature for 24h, then at 80°C for 4h. Samples were then rinsed with deionized distilled water to a neutral pH and oven-dried at 40°C for 48h.

C isotopic analyses. The decarbonated residues were poured into tin capsules (50 to 80 mg of powder) and weighted using a Sartorius M2P ultra-balance before TOC and $\delta^{13}C_{org}$ measurements were performed using a Thermo Fisher Scientific Flash Smart elemental analyser, coupled to a Thermo Fisher Scientific Delta V isotope ratio mass spectrometer (EA-IRMS) via a Conflo IV interface. Certified USGS40 ($\delta^{13}C_{org}$ = -26.39‰, TOC = 40.82 wt.%) and caffeine IAEA-600 ($\delta^{13}C_{org}$ = -27.77‰, TOC = 49.48 wt.%) reference materials were used for the calibration. Total organic carbon (TOC) contents are expressed in dry weight percentage (wt.%) of the non-decarbonated bulk powder and isotope results are reported in delta-notation relative to V-PDB. Each measurement session included three to four standards measurements at the beginning and at the end, as well as one standard measurement every 12 samples. The mean $\delta^{13}C_{org}$ precision for standards is better than 0.35‰ and the mean accuracy better than 0.28‰. Each sample was duplicated. The mean external reproducibility (2σ), based on sample replicate analyses and including powder resampling and reprocessing via chemical treatment, is ± 0.012 wt.% for the TOC content and ± 0.26‰ for the $\delta^{13}C_{org}$.

N isotopic analyses. As all samples contain less than 50 ppm N, the EA-IRMS method applied for carbon analyses is not sensitive enough for reliable bulk nitrogen isotopic analyses[1,48]. Samples were therefore analyzed at IPGP using the "classical sealed-tube combustion method" as described in[1,49]. In brief, N_2 was produced offline through sealed-tube Dumas combustion and cryogenically purified in a vacuum line. Up to 400 mg of decarbonated residual powder was put into a quartz tube with CuO and Cu wires, purified beforehand at 900°C for 2h in a muffle furnace to prevent contamination. Samples were degassed for 12h at 150°C under vacuum to remove adsorbed atmospheric N_2 and organics. Quartz tubes were then sealed directly under vacuum and combusted in a muffle furnace at 950°C for 6h under oxidizing conditions by oxygen liberated from the CuO wires, then cooled at 600°C for 2h, allowing residual oxygen to combine with cupric oxide and nitrous oxide to be reduced by copper, and finally cooled to ambient temperature[50]. The extraction yield for this protocol is 100% for both organic and mineral nitrogen[51], including ammonium in minerals such as phyllosilicates. The content of each quartz tube was released in the vacuum line with a tube cracker, where CO_2 and H_2O were trapped cryogenically to avoid any subsequent isobaric interferences. The purified incondensable N_2 gas was concentrated into a calibrated volume for quantification using a Toepler pump (Hg manometer). Standard analytical procedures for nitrogen usually include CaO in the reagents to trap gaseous CO_2 and H_2O from the samples[50]. Given that the addition of CaO significantly contributes to analytical blanks[51], we performed a few tests which show that the addition of CaO does not yield significant $\delta^{15}N$ differences. Samples were consequently

analyzed without the addition of CaO. Purified N_2 was analyzed by dual-inlet mass spectrometry using a ThermoFinnigan DeltaPlus XP IRMS. Possible air contamination and isobaric interferences (due to CO) were monitored by scanning of m/z 12 (C from CO_2, CO, CH_4 or organic compounds), 18 (H_2O), 30 ($C^{18}O$), 32 (O_2), 40 (atmospheric Ar) and 44 (CO_2). Analytical blanks for the entire procedure are <0.02 micromoles N, which represents a mean of 7% of the gas (17% of the gas for the smallest sample and less than 3% for more concentrated samples). TN and $\delta^{15}N$ values have been individually corrected from the blank contribution, using the reference blank value of $\delta^{15}N$ = -3.7‰[51]. On average, blank-corrected $\delta^{15}N$ values are 2.3‰ higher than their raw counterparts (from 1.2‰ to 3.9‰ higher). External $\delta^{15}N$ reproducibility ranged between 0.1 and 3.5‰ with a mean of 1.5 ± 1.5‰ (n = 6). Samples that were replicated are reported in Table 1. International standards were used in a prior study to calibrate both the EA method and the sealed tube combustion method[52]: it showed that results obtained using the EA-IRMS compared well to those obtained using the sealed tube method presented here. Accuracy was monitored by measuring certified materials IAEA-N1 (+0.4 ± 0.2‰) and IAEA-N2 (+20.3 ± 0.2‰), and IPGP internal standard MS#5 (+14.9 ± 0.5‰)[52]. In addition, samples from the Buck Reef Chert Formation[44], displaying known TN and $\delta^{15}N$ values that strongly differ from the Serra Sul samples, were measured throughout all measurement sessions as internal quality standards.

Geological context of the Serra Sul and Tumbiana formations

Here we present a short description of the geological context of the Serra Sul Formation, Amazonian Craton (Extended Data Figure 3A), and point out the main similarities and differences with the Tumbiana Formation, Pilbara Craton, where similar strongly positive $\delta^{15}N$ values have been reported[5,46]. The age of the Serra Sul Formation is constrained between 2684 ± 10 Ma (U-Pb on detrital zircon[6]) and 2627 ± 11 Ma (Re-Os dating on molybdenite[28]; Extended Data Figure 4). This indicates that the Serra Sul Formation is slightly younger than the Tumbiana Formation, which was deposited around 2724 ± 5 Ma (U-Pb on volcanic zircon)[53] to ≤2715 ± 6 Ma (U-Pb on detrital zircon)[54]. Importantly, paleomagnetic investigations indicate that at about 2.75 Ga the Carajás Basin was located at a low latitude (3.4 ± 8.5°)[32], whereas the Hamersley Basin in which the Tumbiana Formation deposited was located at high to mid paleolatitude (between 51.5 ± 7.0° and 32.1 ± 5.7°)[55]. Both the Serra Sul[6,31,56] and the Tumbiana[57] formations experienced low-grade (≤ 300°C) greenschist facies metamorphism.

The Serra Sul Formation was deposited in the Carajás Basin, southeast Amazonian Craton (Extended Data Figure 3A, B). The basement of the basin comprises various Meso- to Neoarchean rocks[58] capped by a 4 to 6 km thick basaltic series of the ca. 2.75 Ga Parauapebas Large Igneous Province (PLIP)[27]. Soon after the main magmatic pulse of the PLIP, infilling of the rift initiated with the deposition of iron formations (IFs) of the Carajás Formation (Extended Data Figure 4). These IFs are characterized by strong positive Eu anomalies indicating the influence of high-temperature hydrothermal fluids in seawater[59], absence of Ce anomalies arguing for ambient reducing conditions during deposition[59], and occurrence of positive La and Y anomalies[59] typical of chemical sediments deposited in oceanic setting[60]. In addition, Fe and C isotope data indicate that deposition of the IFs was mediated by anoxygenic photosynthetic organisms[59]. The transition from the Carajás to Serra Sul formations is marked by several IFs layers up to 10 m thick, grading upward into detrital terrigenous sedimentary rocks including sandstones, siltstones, conglomerates and flat pebble conglomerates[6,61–65]. The presence of BIFs at the base of the Serra Sul Formation[61] indicates marine environments, and the different

sedimentary features of this formation point toward subaqueous environments ranging from shallow to deep water settings influenced by slope instability and gravity flow processes[6,62,63]. The Serra Sul Formation does not preserve evidence of contemporaneous volcanic activity[6].

These lithologies and environments contrast with those of the Tumbiana Formation, which comprises mainly stromatolitic and fenestrate carbonates, calcareous sandstones, various volcanic and volcaniclastic rocks including tuffs, lapillis and tuffaceous sandstones, and other detrital facies including conglomerates and flat pebbles conglomerates[5,26,46,57,66]. Contrarily to the Serra Sul Formation, the presence of tuffs and lapillis argues for active volcanic activity during the deposition of the Tumbiana Formation[66]. Various sedimentary structures such as desiccation cracks point to shallow subaqueous environments subjected to frequent emersion[26,66]. Geochemical characteristics of chemical sedimentary rocks of the Tumbiana Formation, such as nearly chondritic Y/Ho and the absence of positive Y anomaly, point to lacustrine subaqueous environments[26,66], and strongly positive $\delta^{15}N$ values have been suggested to evidence alkaline waters[5].

Studied drill cores

Samples were collected from two diamond-drilled cores separated by about 1.75 km from each other and intersecting the Serra Sul Formation in the east of the Carajás Basin (Extended Data Figure 3C). These drill cores (GT-41-FURO-13 and GT-41-FURO-16) have been selected due to their low metamorphic and hydrothermal overprints, with only rare occurrences of quartz-chlorite-bearing micro-veins. Both drill cores, named thereafter GT13 and GT16, exhibit similar lithologies and sedimentary facies, but no attempt was made to correlate them, so that their relative stratigraphic positions remain unconstrained. A detailed description of sedimentary facies is presented in ref.[6] and summarized below.

The most common facies association comprises polymictic conglomerates interbedded with sandstones and siltstones with various sedimentary features attesting an overall excellent preservation state (Extended Data Figure 1). This facies association is interpreted to represent deep water environment, where conglomerates and coarse sandstones were deposited by subaqueous mass flow, cohesive debris flow or hyper-concentrated density flow[67–72].

The other facies association identified consists of sandstone, siltstone and flat pebble conglomerates made up of intraclastic granules to pebbles (Extended Data Figure 1). Flat pebble conglomerates are interpreted to result from the failure and subsequent reworking of compacted to loosely consolidated shoreface deposits[73]. The limited transport by mass movement of shoreface deposits and occurrence of wave ripples in sandstones and siltstones suggest relatively shallow water environments (shoreface to upper offshore).

Preservation of the primary N isotope signature

As post-depositional modifications of sedimentary $\delta^{15}N$ can occur during diagenesis and metamorphism, it is essential to evaluate the effects of such processes. It seems unlikely that organic matter remineralization during diagenesis significantly impacted the Serra Sul Formation $\delta^{15}N$ record since early diagenesis under anoxic conditions does not seem to shift organic matter $\delta^{15}N$ values by more than 1‰[74], and the measured values range from +10 to +35‰.

The Serra Sul Formation has undergone metamorphism in the greenschist facies[6]. While an increase in $\delta^{15}N$ and a decrease in TN is usually seen during prograde metamorphism[75–78], studies on coal series show that nitrogen loss from organic matter during anthracitization is not associated with significant $\delta^{15}N$ increase[79–81]. The absence of covariation between $\delta^{15}N$ and TOC/TN in the Serra Sul Formation argues against a strong modification of $\delta^{15}N$ values due to metamorphic N-loss (Extended Data Figure 2). Moreover, maximum isotopic enrichments documented for greenschist facies metamorphism are below 2‰[78,82], which is small compared to the reported range of measured $\delta^{15}N$ in the Serra Sul Formation (between +10‰ and +35‰). Secondary modification of $\delta^{15}N$ values can also occur during metasomatic ammonium addition through hydrothermal recycling, which tends to decrease the TOC/TN and either increase or decrease the $\delta^{15}N$ depending on the isotopic signature of recycled sediments[30,83]. The relative constancy of TOC/TN along the core argues against any heterogeneous secondary overprint of the nitrogen record, either by metamorphism or by metasomatism. Finally, the absence of significant $\delta^{15}N$ differences between facies also argues against a metamorphic or metasomatic modification, as samples of different lithologies would react differently to thermal alteration.

48. Boocock, T. J., Mikhail, S., Prytulak, J., Di Rocco, T. & Stüeken, E. E. Nitrogen Mass Fraction and Stable Isotope Ratios for Fourteen Geological Reference Materials: Evaluating the Applicability of Elemental Analyser Versus Sealed Tube Combustion Methods. *Geostand. Geoanalytical Res.* **44**, 537–551 (2020).

49. Ader, M. *et al.* Ocean redox structure across the Late Neoproterozoic Oxygenation Event: A nitrogen isotope perspective. *Earth Planet. Sci. Lett.* **396**, 1–13 (2014).

50. Kendall, C. & Grim, E. Combustion tube method for measurement of nitrogen isotope ratios using calcium oxide for total rmoval of carbon dioxide and water. *Analytical Chemistry* vol. 62 4 (1990).

51. Busigny, V., Ader, M. & Cartigny, P. Quantification and isotopic analysis of nitrogen in rocks at the ppm level using sealed tube combustion technique: A prelude to the study of altered oceanic crust. *Chem. Geol.* **223**, 249–258 (2005).

52. Fraga-Ferreira, P. L. *et al.* The Nitrogen Cycle in an Epeiric Sea in the Core of Gondwana Supercontinent: A Study on the Ediacaran-Cambrian Bambuí Group, East-central Brazil. *Front. Earth Sci.* **9**, (2021).

53. Blake, T. S., Buick, R., Brown, S. J. A. & Barley, M. E. Geochronology of a Late Archaean flood basalt province in the Pilbara Craton, Australia: constraints on basin evolution, volcanic and sedimentary accumulation, and continental drift rates. *Precambrian Res.* **133**, 143–173 (2004).

54. Arndt, N. T., Nelson, D. R., Compston, W., Trendall, A. F. & Thorne, A. M. The age of the Fortescue Group, Hamersley Basin, Western Australia, from ion microprobe zircon U-Pb results. *Aust. J. Earth Sci.* **38**, 261–281 (1991).

55. Kasbohm, J., Schoene, B., Maclennan, S. A., Evans, D. A. D. & Weiss, B. P. Paleogeography and high-precision geochronology of the Neoarchean Fortescue Group, Pilbara, Western Australia. *Precambrian Res.* **394**, 107114 (2023).

56. Martins, P. L. G. *et al.* Neoarchean magmatism in the southeastern Amazonian Craton, Brazil: Petrography, geochemistry and tectonic significance of basalts from the Carajás Basin. *Precambrian Res.* **302**, 340–357 (2017).

57. Lepot, K., Benzerara, K., Brown, G. E. & Philippot, P. Microbially influenced formation of 2,724-million-year-old stromatolites. *Nat. Geosci.* **1**, 118–121 (2008).

58. Vasquez, M. L. & Rosa-Costa, L. T. da. *Geologia e recursos minerais do estado do Pará*. http://rigeo.sgb.gov.br/jspui/handle/doc/10443 (2008).

59. Rego, E. S. *et al.* Anoxygenic photosynthesis linked to Neoarchean iron formations in Carajás (Brazil). *Geobiology* **19**, 326–341 (2021).

60. Kamber, B. S., Webb, G. E. & Gallagher, M. The rare earth element signal in Archaean microbial carbonate: information on ocean redox and biogenicity. *J. Geol. Soc.* **171**, 745–763 (2014).

61. Melo, G. H. C. de *et al.* Evolution of the Igarapé Bahia Cu-Au deposit, Carajás Province (Brazil): Early syngenetic chalcopyrite overprinted by IOCG mineralization. *Ore Geol. Rev.* **111**, 102993 (2019).

62. Dreher, A. M., Xavier, R. P. & Martini, S. L. Fragmental rocks of the Igarapé Bahia CU-AU deposit, Carajas Mineral Province, Brazil. *Rev. Bras. Geociências* **35**, 359–368 (2005).

63. Dreher, A. M., Xavier, R. P., Taylor, B. E. & Martini, S. L. New geologic, fluid inclusion and stable isotope studies on the controversial Igarapé Bahia Cu–Au deposit, Carajás Province, Brazil. *Miner. Deposita* **43**, 161–184 (2008).

64. Galarza, M. A., Macambira, M. J. B. & Villas, R. N. Dating and isotopic characteristics (Pb and S) of the Fe oxide–Cu–Au–U–REE Igarapé Bahia ore deposit, Carajás mineral province, Pará state, Brazil. *J. South Am. Earth Sci.* **25**, 377–397 (2008).

65. Ronzê, P. C., Soares, A. D., Santos, M. dos & Barreira, C. F. Alemão copper-gold (U-REE) deposit, Carajás, Brazil. *Hydrothermal Iron Oxide Copp.-Gold Relat. Depos. Glob. Perspect. Aust. Miner. Found. Adel.* 191–202 (2000).

66. Coffey, J. M., Flannery, D. T., Walter, M. R. & George, S. C. Sedimentology, stratigraphy and geochemistry of a stromatolite biofacies in the 2.72 Ga Tumbiana Formation, Fortescue Group, Western Australia. *Precambrian Res.* **236**, 282–296 (2013).

67. Lowe, D. R. Sediment gravity flows; II, Depositional models with special reference to the deposits of high-density turbidity currents. *J. Sediment. Res.* **52**, 279–297 (1982).

68. Mulder, T. & Alexander, J. The physical character of subaqueous sedimentary density flows and their deposits. *Sedimentology* **48**, 269–299 (2001).

69. Nemec, W. & Steel, R. J. Alluvial and Coastal Conglomerates: Their Significant Features and Some Comments on Gravelly Mass-Flow Deposits. 1–31 (1984).

70. Postma, G., Kleverlaan, K. & Cartigny, M. J. B. Recognition of cyclic steps in sandy and gravelly turbidite sequences, and consequences for the Bouma facies model. *Sedimentology* **61**, 2268–2290 (2014).

71. Postma, G. & Cartigny, M. J. B. Supercritical and subcritical turbidity currents and their deposits—A synthesis. *Geology* **42**, 987–990 (2014).

72. Walker, R. G. Generalized Facies Models for Resedimented Conglomerates of Turbidite Association. *GSA Bull.* **86**, 737–748 (1975).

73. Myrow, P. M. *et al.* Flat-pebble conglomerate: its multiple origins and relationship to metre-scale depositional cycles. *Sedimentology* **51**, 973–996 (2004).

74. Lehmann, M. F., Bernasconi, S. M., Barbieri, A. & McKenzie, J. A. Preservation of organic matter and alteration of its carbon and nitrogen isotope composition during simulated and in situ early sedimentary diagenesis. *Geochim. Cosmochim. Acta* **66**, 3573–3584 (2002).

75. Bebout, G. E. & Fogel, M. L. Nitrogen-isotope compositions of metasedimentary rocks in the Catalina Schist, California: Implications for metamorphic devolatilization history. *Geochim. Cosmochim. Acta* **56**, 2839–2849 (1992).

76. Boyd, S. R. & Philippot, P. Precambrian ammonium biogeochemistry: a study of the Moine metasediments, Scotland. *Chem. Geol.* **144**, 257–268 (1998).

77. Haendel, D., Mühle, K., Nitzsche, H.-M., Stiehl, G. & Wand, U. Isotopic variations of the fixed nitrogen in metamorphic rocks. *Geochim. Cosmochim. Acta* **50**, 749–758 (1986).

78. Jia, Y. Nitrogen isotope fractionations during progressive metamorphism: A case study from the Paleozoic Cooma metasedimentary complex, southeastern Australia. *Geochim. Cosmochim. Acta* **70**, 5201–5214 (2006).

79. Ader, M., Boudou, J.-P., Javoy, M., Goffe, B. & Daniels, E. Isotope study on organic nitrogen of Westphalian anthracites from the Western Middle field of Pennsylvania (U.S.A.) and from the Bramsche Massif (Germany). *Org. Geochem.* **29**, 315–323 (1998).

80. Ader, M. *et al.* Nitrogen isotopic evolution of carbonaceous matter during metamorphism: Methodology and preliminary results. *Chem. Geol.* **232**, 152–169 (2006).

81. Boudou, J.-P. *et al.* Organic nitrogen chemistry during low-grade metamorphism. *Geochim. Cosmochim. Acta* **72**, 1199–1221 (2008).

82. Stüeken, E. E., Zaloumis, J., Meixnerová, J. & Buick, R. Differential metamorphic effects on nitrogen isotopes in kerogen extracts and bulk rocks. *Geochim. Cosmochim. Acta* **217**, 80–94 (2017).

83. Stüeken, E. E., Gregory, D. D., Mukherjee, I. & McGoldrick, P. Sedimentary exhalative venting of bioavailable nitrogen into the early ocean. *Earth Planet. Sci. Lett.* **565**, 116963 (2021).

84. Cordani, U. G. *et al.* Tectonic map of South America=Mapa tectônico da América do Sul. (2016).

85. Vasquez, M. L., Sousa, C. S. & Carvalho, J. M. A. Mapa geológico e de recursos minerais do Estado do Pará, escala 1: 1.000. 000. *Programa Geol. Bras. Belém CPRM* (2008).

86. Machado, N., Lindenmayer, Z., Krogh, T. E. & Lindenmayer, D. U-Pb geochronology of Archean magmatism and basement reactivation in the Carajás area, Amazon shield, Brazil. *Precambrian Res.* **49**, 329–354 (1991).

87. Trendall, A. F., Basei, M. A. S., de Laeter, J. R. & Nelson, D. R. SHRIMP zircon U–Pb constraints on the age of the Carajás formation, Grão ParáGroup, Amazon Craton. *J. South Am. Earth Sci.* **11**, 265–277 (1998).

88. Rossignol, C. *et al.* Neoarchean environments associated with the emplacement of a large igneous province: Insights from the Carajás Basin, Amazonia Craton. *J. South Am. Earth Sci.* **130**, 104574 (2023).

Acknowledgments

For technical support, the authors would like to thank Anne-Lise Santoni and the GISMO platform (Université de Bourgogne, France), and Guillaume Landais, Romaric Tchibinda, Gerard Bardoux and Virginia Rojas (Institut de Physique du Globe de Paris, France).

Funding

Institut Universitaire de France (IUF) – project EVOLINES (CT)

Observatoire des Sciences de l'Univers Terre Homme Environnement Temps Astronomie of Bourgogne-Franche-Comté (OSU THETA) – project NITROPAST (CT)

Fundação de Amparo à Pesquisa do Estado de São Paulo, FAPESP Projects 2019/16271-0; 2018/05892-0; 2015/16235-2; 2018/02645-2; 2019/16066-7 (PP)

Author contributions

Conceptualization: AP, CT, MA, PP

Investigation: AP

Funding acquisition: CT, PP

Supervision: CT, MA

Writing – original draft: AP

Review & editing: AP, CT, MA, VB, ER, CR, PP

Competing interests

Authors declare that they have no competing interests.

Data and materials availability

All data are available in the main text or the supplementary materials.

EXTENDED DATA ITEMS

Extended Data Figure 1. Sedimentological logs of the drill cores GT13 and GT16 with photographs of the main facies and sedimentary structures. Arrows point to the stratigraphic top. Top left photograph: conglomerate with oriented clasts and sandy matrix; middle left: alternations of siltstone and fine sandstone; bottom left and middle: syn-sedimentary, centimetric-scale faults within fine sandstone to siltstone. Top right: sandstone with wave ripples, framboidal pyrite (blue circles) and load casts. Middle right: normally graded conglomerate with rounded quartz pebbles and sub-angular sedimentary clasts, grading to coarse sandstone. Bottom right: flat pebble conglomerate comprising elongated and deformed intraformational clasts.

Extended Data Figure 2. Crossplots for drill cores GT13 (orange) and GT16 (red): TOC (wt. %) vs. TN (ppm); $\delta^{15}N$ (‰ vs. air) vs. TN (ppm); $\delta^{15}N$ (‰ vs. air) vs. TOC/TN and $\delta^{13}C_{org}$ (‰ vs. PDB) vs. $\delta^{15}N$ (‰ vs. air).

Extended Data Figure 3. Maps illustrating the location of the Carajás Basin. a, Main tectonic elements of South America[84]. **b,** Geological map of the Carajás Basin[85]. **c,** Location of the drill cores.

Extended Data Figure 4. Main sedimentary units of the Carajás Basin and age constraints. 1: ref.[86]; 2, 3: ref.[87]; 4: ref.[88]; 5: ref.[6]; 6: ref.[28].

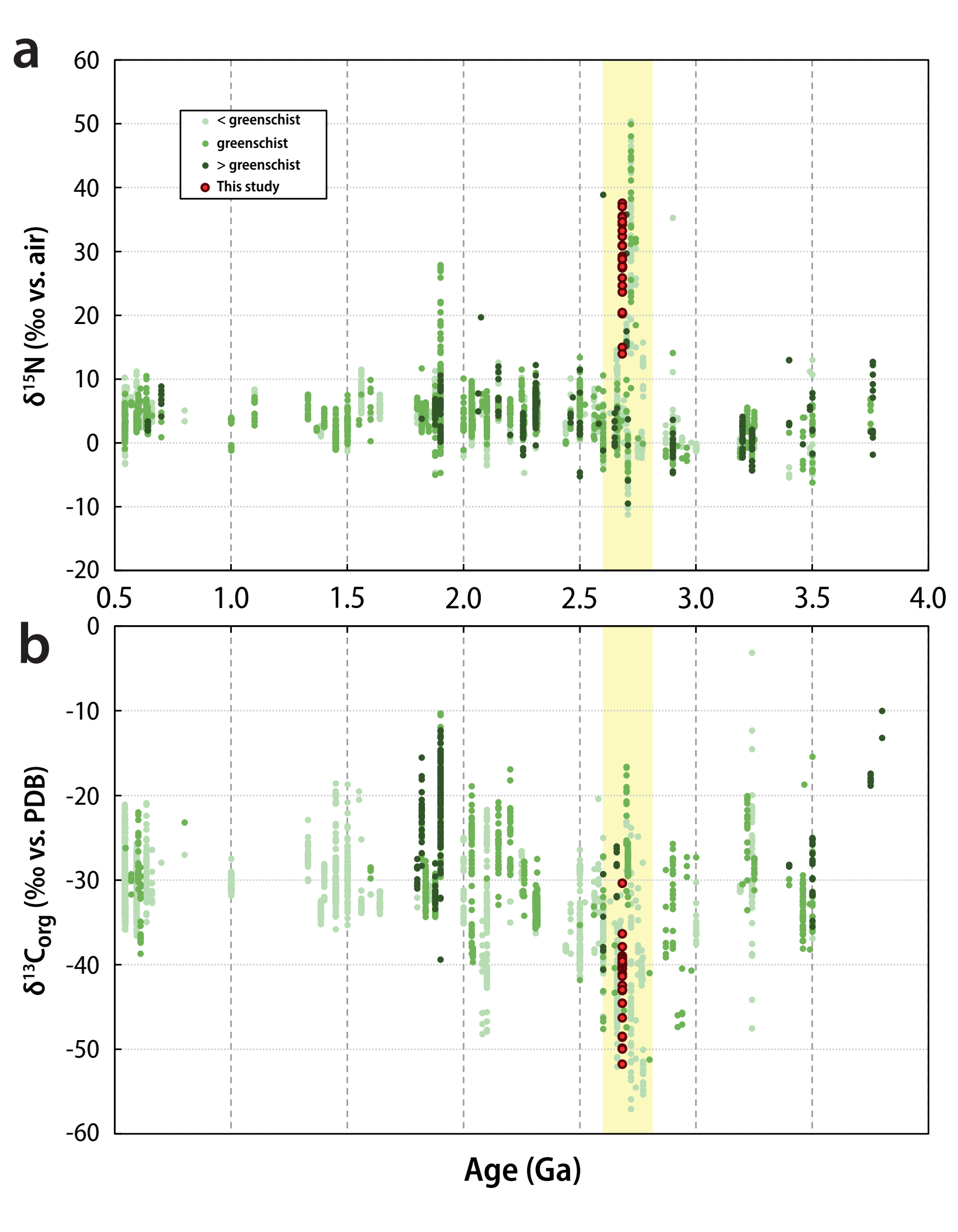
a
b
< greenschist
greenschist
> greenschist
This study
δ15N (‰ vs. air)
δ13Corg (‰ vs. PDB)
Age (Ga)
60
50
40
30
20
10
0
-10
-20
0.5
1.0
1.5
2.0
2.5
3.0
3.5
4.0
-30
-40
-50
-60

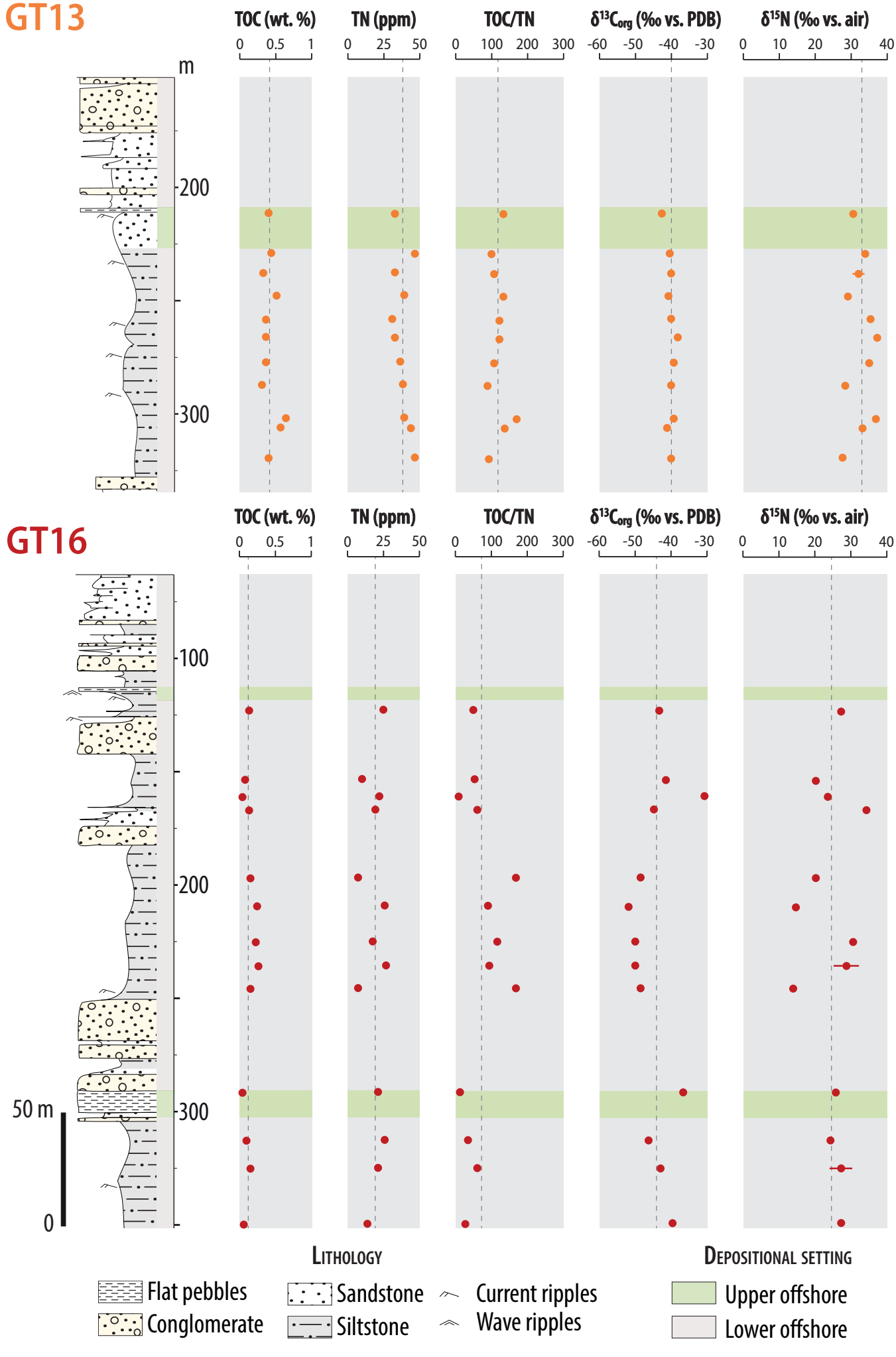
GT13
TOC (wt. %)
0 0.5 1
TN (ppm)
0 25 50
TOC/TN
0 100 200 300
δ13Corg (‰ vs. PDB)
-60 -50 -40 -30
δ15N (‰ vs. air)
0 10 20 30 40
m
200
300
GT16
TOC (wt. %)
0 0.5 1
TN (ppm)
0 25 50
TOC/TN
0 100 200 300
δ13Corg (‰ vs. PDB)
-60 -50 -40 -30
δ15N (‰ vs. air)
0 10 20 30 40
100
200
300
50 m
0
Lithology
Flat pebbles
Conglomerate
Sandstone
Siltstone
Current ripples
Wave ripples
Depositional setting
Upper offshore
Lower offshore